PAPER

Check for updates

Galena weathering under simulated acid rain conditions: electrochemical processes and environmental assessments

Kai Zheng,[ab] Heping Li,[a] Luying Wang,[ab] Xiaoying Wen[a] and Qingyou Liu [iD] *[a]

Galena can be easily weathered under acid rain conditions and causes environmental issues. This process, in nature, is an electrochemical process. *In situ* electrochemical technology and surface analysis technology were combined to investigate this weathering process. The experimental results showed that galena weathering under simulated acid rain (SAR) could cause an initial increase in Pb^{2+} ions and result in the formation of a passive S^0 film, and the terminal product was SO_4^{2-}. Increased acidity stimulates galena weathering, and the promotion efficiency was 2208% as the pH of the SAR decreased from 5.2 to 4.2. The presence of pyrite is favourable for galena weathering, and the promotion efficiency was 150% when contained 25% (wt%) pyrite. Galena will release 1.7 g per m^2 per year Pb^{2+} to solution when the pH of acid rain is 5.2, and the released Pb^{2+} will reach 95.7 g per m^2 per year when the pH of acid rain is 4.2 plus the galvanic effect of pyrite.

Environmental significance

In the manuscript, we present the results and conclusions from a study of galena weathering behaviors under simulated acid rain. Our study is one of the few that combine *in situ* electrochemical technology with surface analyses to investigate galena weathering behaviors. By combining the two methods, it is possible to identify how acid rain and associated mineral pyrite affect the galena weathering process. The results show galena will release 1.7 g per m^2 per year Pb^{2+} to solution when the pH of acid rain is 5.2, and the released Pb^{2+} will reach 95.7 g per m^2 per year when the pH of acid rain is 4.2 plus the galvanic effect of pyrite. By combining the two methods we can identify the weathering process of other electrically conductive minerals under natural conditions, which is valuable for the quantitative evaluation of environmental pollution caused by the weathering process of other electrically conductive minerals.

1 Introduction

Galena (PbS) is one of the most common metal sulfide minerals and can be easily weathered (oxidized) during geochemical processes or by human exploitation. These processes may release Pb^{2+} and other heavy metal ions (such as Zn, As and Cd), which results in heavy metal environmental issues. Lar *et al.* noted that the release of Pb and other potentially harmful elements from galena mining activities has significantly contributed to the enrichment of these elements in the surrounding environment.[1] The heavy metals Pb, Zn and Cd in Jebel Ressas (NE Tunisia) soil are severe and exceed the environmental norms, as large volumes of Pb–Zn flotation tailings are eroded by wind and running waters. During the past several years, the Deûle River (France) fluvial environment has experienced severe degradation.[2] Boughriet *et al.* indicated that the Metaleurop smelting plant was the major culprit of the

degradation because the smelter inputs contain sulfidic ores in the sulfide/organic fraction, which results in galena (PbS), wurtzite (ZnS) and pyrite (FeS_2) in the Deule River sediment.[3]

Acid rain (acidic deposition) is caused by SO_2 emissions (principally from fossil-fuel power stations, metal smelters and other stationary sources) and NO_x (from mobile sources, industrial sources and power plants) that form sulfuric and nitric acid, respectively, in precipitation. In 1872, Smith conducted detailed studies of acid rain and described many of its potentially harmful effects.[4] Over the past several decades, many regions, including Europe, eastern North America, Southeast Asia, and especially central and southern China, have suffered from the effects of acidic deposition.[5] As a major international environmental issue, acid rain may have harmful effects on ecosystems,[6] soils and soil water,[7] aquatic ecosystems,[8,9] materials,[10] and even human health.[11]

Natural galena, which includes raw ore and lead/zinc mine tailings that contain galena, is often seen at the crust surface or in the shallow crust and may thereby suffer from acid rain weathering. For example, the three large, well-known Pb–Zn deposit mines in China, Fankou (Guangdong Province), Jinding and Dongchuan (Yunnan Province), all lie in serious acid rain

[a] Key Laboratory of High-temperature and High-pressure Study of the Earth's Interior, Institute of Geochemistry, Chinese Academy of Sciences, Guiyang 550081, China. E-mail: liuqingyou@vip.gyig.ac.cn

[b] University of Chinese Academy of Sciences, Beijing, 100039, China

This journal is © The Royal Society of Chemistry 2018

areas.[12] Generally, acid rain will accelerate the rate of acidification and worsen environmental pollution by heavy metal ions.[13] Hence, many investigations have concentrated on the impacts of acid rain on sulfide ore (including galena) weathering. Under natural conditions, acid rain and rain affect the secondary sulfide mineral assemblages and acid mine drainage. Smuda et al. studied a sulfide-rich (including galena, pyrite and sphalerite) waste rock dump.[14] The results showed that the concentrations of Cu, Zn and Pb differed in the primary mineral assemblage and secondary mineral enrichment. Rain events cause the dissolution of most efflorescent salts, remove the enrichment at the base and result in a washout of acidic solutions rich in heavy metal ions. Moreover, rains affect the geochemical sulfide dynamics. Chavez et al. investigated several metal sulfide ore deposits in central Mexico and found that the redox reactions locally produce a pH of approximately 2.0 in leachates with high metal contents.[15] Furthermore, the geochemical dynamics of the sulfides were controlled by seasonal rains (from June to September), along with high evaporation rates. These factors resulted in minor acid mine drainage and metal leaching. Redox and dissolution–precipitation reactions control the mobility of heavy metals in the surrounding environment and pose a threat to the local population. Acid rain affects the mobility and speciation of metals in lead/zinc tailing soil. Ding et al. used simulated acid rain (SAR) to leach a typical lead/zinc tailing soil and revealed that Zn was predominantly associated with the acid extractable and residual fractions, Pb was predominantly associated with the reducible fraction, and Cu was dominant in the reducible and oxidizable fractions.[16] Yuan and Liu used simulated acid rain leaching to investigate a mine tailing (the main minerals were galena and sphalerite). They revealed that the migration of heavy metals in lead and zinc mine tailings would be greatly enhanced under acid leaching conditions, Pb and Zn were mainly present in the residual fraction, and a greater solid–liquid ratio and lower acid rain pH contributed to higher leaching concentrations of heavy metals.[17]

Galena is one of the metal sulfide minerals that has semiconductor properties, and galena weathering is an electrochemical process in nature.[18] Until recently, geologists were not concerned about galena weathering from an electrochemical corrosion viewpoint, especially considering the lack of quantitative data in this field. Therefore, in this study, the electrochemical corrosion of galena (including galena containing pyrite to investigate galvanic effects) in simulated acid rain was studied in Dongchuan. Dongchuan is a Pb–Zn mine area in Yunnan Province, China that experiences serious acid rain pollution. The primary objectives of this study were as follows: (1) to understand the response of the galena weathering mechanism to acid rain and (2) to investigate the effects of acid rain on galena weathering.

2   Materials and methods

2.1   Mineral electrode preparation

Galena and pyrite samples were collected from the Dongchuan Pb–Zn mine (Yunnan Province, China). Reflected light microscopy and X-ray diffraction analysis indicated that the samples existed in a pure, homogeneous phase. Electron microprobe analysis confirmed that the concentrations of Fe and S (wt%) in the pyrite sample were 46.89% and 52.96%, respectively, and the contents of Pb, S and Zn (wt%) in the galena sample were 86.53%, 13.39% and 0.0064%, respectively. First, the large galena and pyrite samples were crushed to smaller than 4 mm and then carefully selected by hand. Next, the samples were rinsed with a 3% (v/v) acidic solution, washed with deionized water and dried under vacuum in an attempt to remove the surficial oxide phases formed during sample handling. The resulting galena and pyrite samples were then ground in an agate mortar and sieved to obtain sizes of <74 μm.

One objective of this work was to investigate how pyrite affects the oxidation behaviour of galena; thus, it was critical to prepare the working electrode with both galena and pyrite. Sawyer and Roberts utilized a carbon paste electrode (CPE) and found that it had both good selectivity and sensitivity and did not require several conditioning steps before the analytical measurements, and it was also suitable, versatile and rapid enough for multicomponent determinations.[19] In practice, many researchers have used CPE–mineral electrodes and revealed that CPEs are useful in both mineral kinetic and thermodynamic oxidation studies of sulfide.[20,21] In this work, galena and pyrite carbon paste electrodes were used as the working electrodes, where 0.8 g of graphite (microcrystal grade, APS 2–15 micron, metal basis 99.9995% l Fisher Scientific UK Ltd, Alfa Aesar) and 1.2 g of an electroactive mineral, (1) PbS 1.2 g, (2) PbS 0.9 g + FeS$_2$ 0.3 g, and (3) FeS$_2$ 1.2 g, were mixed together in an agate mortar, and then, 1.0 mL of silicone oil (CAS 63148-52-7, Sigma-Aldrich Co. LLC) was added to obtain a homogeneous paste. This paste was placed in a 3 cm long, 0.5 cm diameter polytetrafluoroethylene syringe and pushed out of the tube with a plunger to renew the surface after each experiment. The surface area was measured to be 0.0196 cm^2. Electrical contact was achieved with a platinum wire immersed in the paste. Further details regarding these electrodes can be found in Lazaro et al.[22]

2.2   Simulated acid rain

According to acid rain monitoring data from 2005 to 2011 in China, the acid rain type was mainly sulfuric acid, and the contribution of nitrate to the acidity of precipitation increased year after year. The annual average pH value was at the same level as that in the USA, Japan and other East Asian countries. However, the deposition flux of the major acidic ions was at a higher level, especially in Dongchuan (Yunnan Province, China), which is one of the areas with the most serious acid rain.[12] According to the monitoring data from the Dongchuan Environmental Monitoring Station, the average pH of the rain in Dongchuan ranged from 4.42 to 6.51 from 2006 to 2013, and the average concentration (mol L^{-1}) ratio of SO$_4^{2-}$ to NO$_3^-$ was 3.39 : 1.[23] To simulate the acid rain characteristics in Dongchuan, China as per the above analysis, first, a dilute solution containing CaSO$_4$, (NH$_4$)$_2$SO$_4$, MgSO$_4$, NaNO$_3$, NH$_4$Cl, NaCl and KF with a molar ratio of 20 : 9 : 5 : 10 : 2 : 2 : 4 was prepared,

This journal is © The Royal Society of Chemistry 2018

Environ. Sci.: Processes Impacts, 2018, **20**, 822–832 | 823

Table 1 Ion concentrations of simulated acid rain (μmol L^{-1})

	pH	Ca^{2+}	Mg^{2+}	NH$_4^+$	K$^+$	Na$^+$	Cl$^-$	F$^-$	SO$_4^{2-}$	NO$_3^-$
SAR1	5.2	40	10	40	8	24	8	8	70	21
SAR2	4.2	40	10	40	8	24	8	8	95	28

and the molar ratio of SO$_4^{2-}$: NO$_3^-$ was 3.39 : 1. Then, two types of acid rain (pH 5.2 and 4.2) were prepared by adjusting the pH of the solution with a solution containing H$_2$SO$_4$ and HNO$_3$ at a molar ratio of SO$_4^{2-}$ to NO$_3^-$ of 3.39 : 1. The details of the ion compositions of the SAR are listed in Table 1.

2.3 Electrochemical studies

Electrochemical measurements were performed using a computer-controlled electrochemical measurement system (PARSTAT 2273, Princeton Applied Research) with a conventional three-electrode electrolytic cell that included a platinum auxiliary electrode, mineral carbon paste electrode (working electrode) and a saturated calomel reference electrode (SCE). All other potentials in this study are quoted relative to the SCE (0.242 V $vs.$ the standard hydrogen electrode) unless stated otherwise. To minimize the resistance of the solution between the working electrode and the reference electrode, the reference electrode was connected to a Luggin capillary.

A 25 mL SAR electrolyte solution at either pH 5.2 or pH 4.2 (refer to Section 2.2) was used in each test. The working, auxiliary and reference electrodes were situated in the same location to ensure a uniform spatial relationship. The experiments were conducted in a water bath at 25 $\pm$ 1 °C.

Cyclic voltammetry (CV) experiments were conducted at a scan rate of 5 mV s^{-1}. The sweeps were initiated in the positive-going direction. The potential started from the open circuit potential (OCP) to 0.9 V ($E_{\lambda a}$ $vs.$ SCE), then reverse scanned to -0.9 V ($E_{\lambda c}$ $vs.$ SCE), and finally returned to the OCP as the final potential (E_f). Polarization curves were obtained by automatically changing the electrode potential from -250 to

$+250$ mV ($vs.$ OCP) at a scan rate of 10 mV s^{-1}. Identical experiments were repeated at least three times to ensure that the reported results were reproducible ($i.e.$, the random errors of the three identical experimental results were within the tolerance limits), and all of the reported results in this study were averaged.

Prior to the CV and polarization curve tests, OCP tests were performed. During the OCP test, the electrode potential increased for 10 min and then reached a quasi-steady state. The steady-state is defined here as a change of less than 2 mV per 5 min. Then, the electrode was stabilized for 400 s, and the potential was recorded as the OCP. During the second and third identical experiments, if the potential was not within ±5 mV (compared with the first test) at the quasi-steady state, then the OCP test was terminated, and a new test was performed until an OCP that was the same as the first test was obtained when stabilized for $\sim$400 s.

2.4 Surface analysis

All galena samples with/without pyrite, after 2 weeks and 10 weeks of weathering under pH 4.2 or 5.2 SAR conditions, were characterized via scanning electron microscopy (SEM) using an X-ray spectrometer produced by EDAX, and a low/high vacuum and digital scanning electron microscopy (JSM-6460LV) were used for chemical analysis (SEM-EDS analysis). Furthermore, all Raman spectra were recorded using a British Renishaw inVia Reflex type microscopic confocal laser Raman spectrometer (laser wavelength λ = 514 nm, exposure time 10 s, and laser power 50 mW). Under these conditions, no laser damage occurred to the galena.

3 Results and discussion

3.1 Open circuit potential study

The open circuit potential (equilibrium potential or rest potential) of a sulfide mineral electrode is a mixed potential, which consists of the cathodic reduction of dissolved oxygen and the anodic oxidation of the mineral surface.[24] Accordingly, the electrochemical behaviour of the mineral surface can be
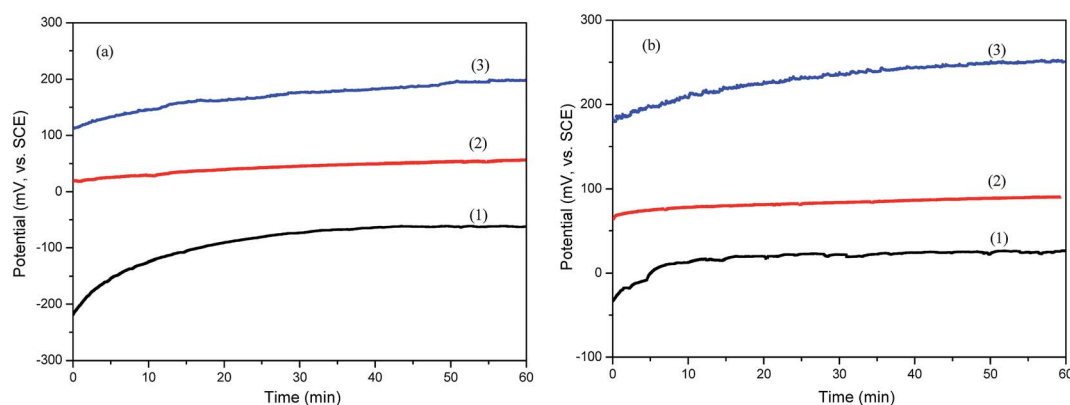

Fig. 1 Potential–time relationships of different mineral electrodes in pH 5.2 (a) and pH 4.2 (b) SARs. (1) CPE–galena, (2) CPE–galena–pyrite and (3) CPE–pyrite.

Table 2 The OCP of galena electrodes containing different mass fractions of pyrite (wt%)

Electrode	OCP (vs. SCE, ±5 mV)	
	pH 5.2 SAR	pH 4.2 SAR
CPE–PbS	−60.3	25.4
CPE–PbS–FeS$_2$ (25%)	55.6	90.2
CPE–FeS$_2$	200.5	250.8

easily evaluated using OCP measurements. The OCP curves of the mineral electrodes under different simulated acid rain conditions are shown in Fig. 1.

Fig. 1(a) shows the OCP curves of the galena electrodes with different mass fractions of pyrite in the pH 5.2 SAR solutions as a function of time. Approximately 40 min after initiation, the potential of the galena electrode reached a quasi-steady state (varied by less than 2 mV min^{-1}), which indicates the spontaneous growth of a passive film on the surface of the electrodes. This time was taken as the preconditioned surface time.[25] For the galena electrode, the OCP was approximately −60.3 ± 5 mV.

The pyrite electrode had a similar potential–time profile, and only the OCP value at 200.5 ± 5 mV was different, which is consistent with the fact that pyrite has a high rest potential.[26] When the pyrite content of the galena electrode was 25% (wt%), we observed a similar potential–time profile, and the OCP was 55.6 ± 5 mV between the galena and the pyrite electrodes, which agrees with the mixed potential theory.[27]

Fig. 1(b) shows the OCP curves of the galena electrodes with different mass fractions of pyrite in the pH 4.2 SAR solutions as a function of time. All three potential–time profiles are similar to those in the pH 5.2 SAR solutions, except that the quasi-steady time is shorter, and the OCP is larger in the pH 4.2 SAR solutions. Similar to that in the pH 5.2 SAR solutions, the OCP order is galena < mixed < pyrite. Compared to the results in the pH 5.2 SAR solutions with the same electrode (galena, pyrite or mixed electrode), the quasi-steady time decreased as the concentration of H$^+$ increased, which revealed that H$^+$ confirmed a galena or pyrite electrochemical interaction. Furthermore, the increase in the OCP with the increase in the H$^+$ concentration can be explained by the cathodic reduction of dissolved oxygen as mentioned above; that is, O$_2$ + 4H$^+$ + 4e$^-$ = 2H$_2$O. Clearly, the higher H$^+$ concentration promoted a cathodic reduction and
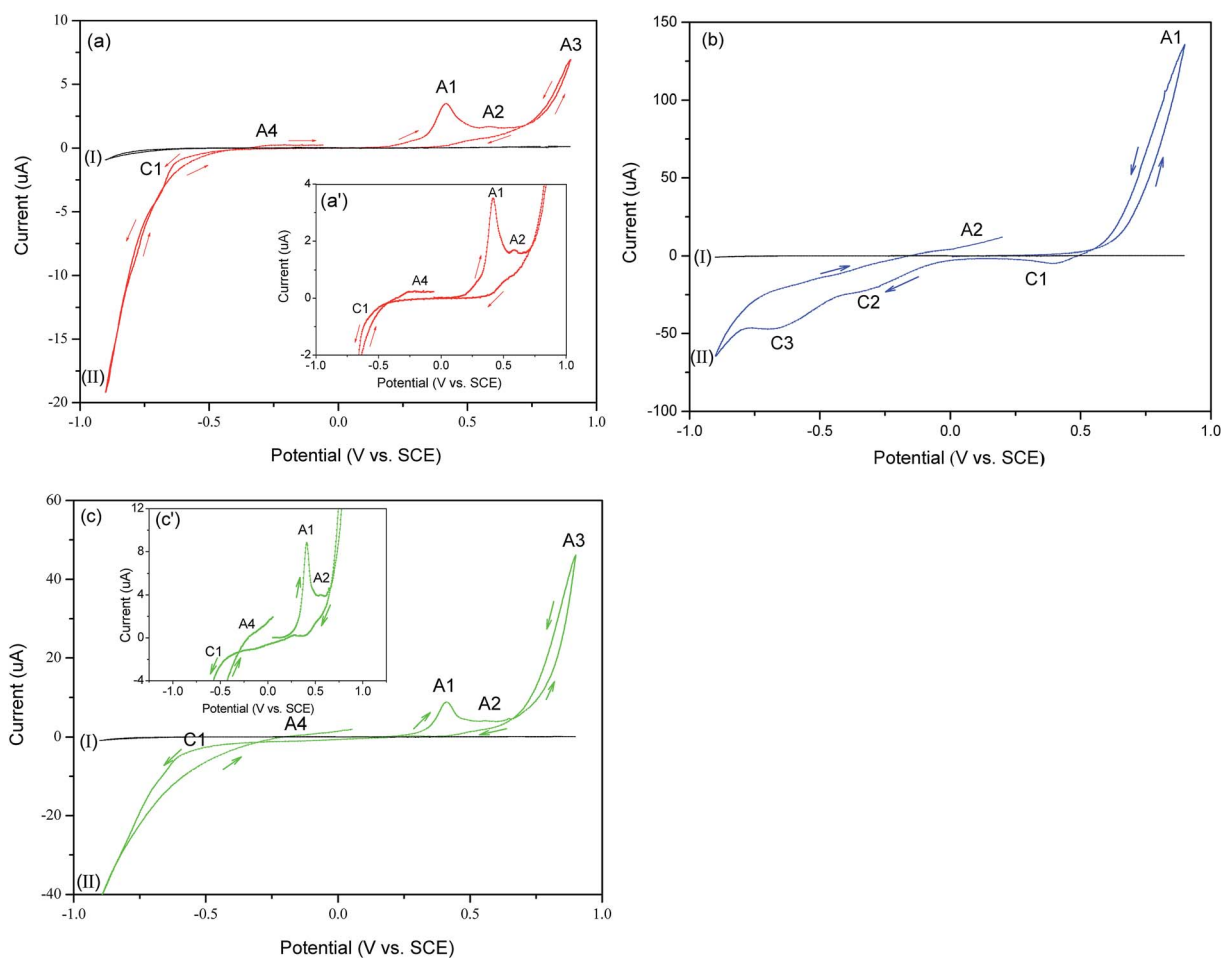

Fig. 2 Typical cyclic voltammogram profiles of CPE-without mineral(I) and CPE−mineral(II) in pH 5.2 SAR. (a) CPE−galena, (b) CPE−pyrite and (c) CPE−galena−pyrite. $E_i = E_{OC}$, $E_{\lambda a} = 0.9$ V, $E_{\lambda c} = -0.9$ V, $E_f = E_{OC}$, $v = 5$ mV S^{-1}. Where (a′) and (c′) are re-scaled versions of (a) and (c) at the same image, respectively.

This journal is © The Royal Society of Chemistry 2018

Environ. Sci.: Processes Impacts, 2018, **20**, 822–832 | 825

thus an increase in the OCP. The detailed OCP values of the different mineral electrodes are listed in Table 2.
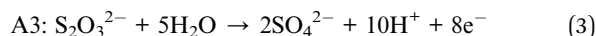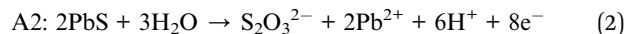
3.2 Cyclic voltammetry studies

Cyclic voltammetry has been widely used for sulfide mineral oxidation studies. In this work, cyclic voltammetry was applied to a variety of redox processes and was used to determine the presence of intermediates in redox reactions. The CPE voltammograms containing PbS and/or FeS$_2$ in the pH 5.2 SAR solutions are shown in Fig. 2.
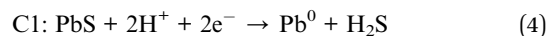
Fig. 2(a) shows the cyclic voltammogram obtained from the CPE–galena with the sweep potential starting from the OCP. During the potential positive-going scan, the oxidation rate quickly increased, and the first anodic maximum (A1) was detected at a potential of ∼0.4 V $vs.$ SCE, which is consistent with the results (0.3–0.5 V) from Paul $et\ al.$[20] In addition, the peak corresponded to the anodic dissolution of galena.

$$A1: PbS \rightarrow Pb^{2+} + S^0 + 2e^- \tag{1}$$
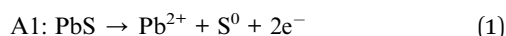
A small peak, A2, was observed near 0.5 V. This peak was tentatively attributed to the transformation of PbS into intermediate S$_2$O$_3^{2-}$ at a higher positive potential via the reaction (2).[28,29] After the potential was scanned to 0.9 V ($E_{\lambda a}$), a third anodic peak (A3) emerged. Almeida and Giannetti suggested that the peak may be associated with the intermediate S$_2$O$_3^{2-}$ being transformed into steady-state sulfate.[30]

$$A2: 2PbS + 3H_2O \rightarrow S_2O_3^{2-} + 2Pb^{2+} + 6H^+ + 8e^- \tag{2}$$

$$A3: S_2O_3^{2-} + 5H_2O \rightarrow 2SO_4^{2-} + 10H^+ + 8e^- \tag{3}$$

In the reverse scan, only one cathodic current peak was observed at a potential between −0.6 V and −0.8 V. The current peak (C1) may correspond to the direct reduction of galena, as indicated in reaction (4).[31] In contrast, Sivenas and Foulkes also reported that the peak corresponding to the reduction of Pb^{2+} did not appear due to the presence of SO$_4^{2-}$ (one is from reaction (3), and another is from the SAR solution).[32] The Pb^{2+} ions were consumed in the form of insoluble PbSO$_4$.

$$C1: PbS + 2H^+ + 2e^- \rightarrow Pb^0 + H_2S \tag{4}$$

As the sweep reversed and continued in the anodic direction, an oxidation peak, A4, was observed from −0.45 to −0.35 V. This peak corresponded to the oxidative dissolution of elemental Pb^0 previously formed via reaction (4), which is in agreement with the results of Sivenas and Foulkes.[32]
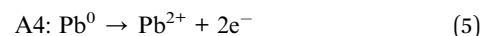
$$A4: Pb^0 \rightarrow Pb^{2+} + 2e^- \tag{5}$$

Fig. 2(b) shows the cyclic voltammogram obtained from the CPE–pyrite with the sweep potential starting from the OCP. The resulting curve is similar to those reported in the literature.[30–33] During the potential positive-going scan, the oxidation rate quickly increases, and the A1 anodic current peak is observed.
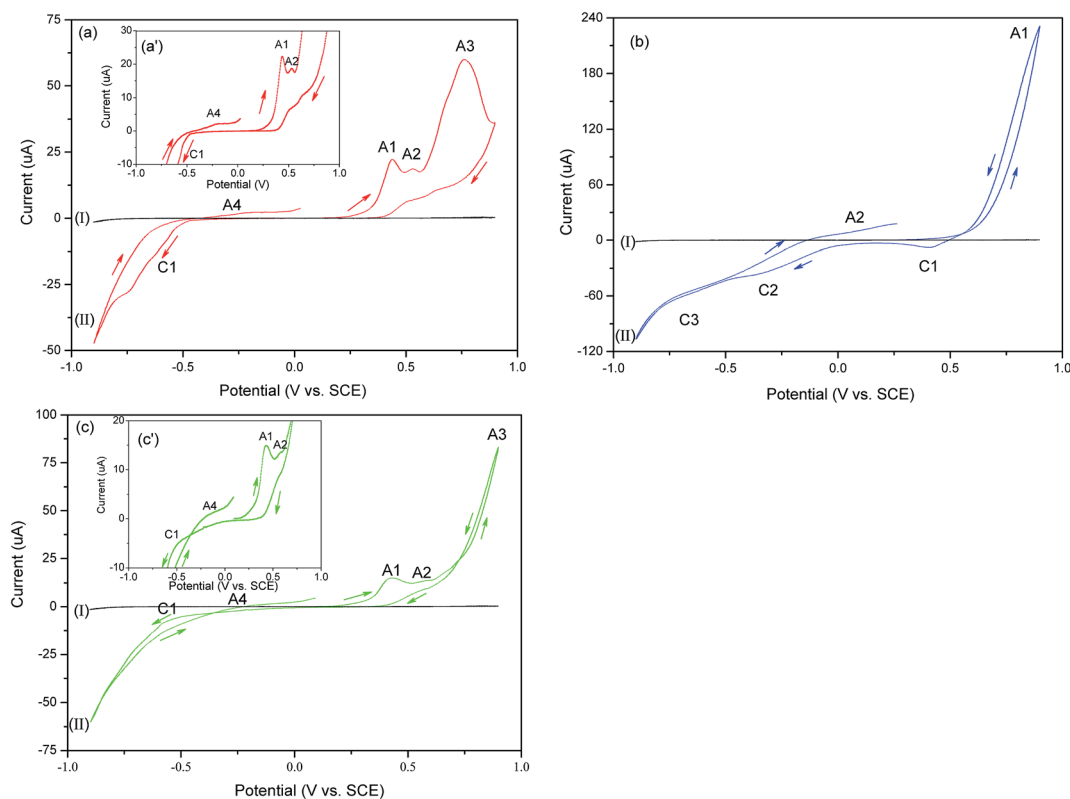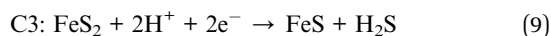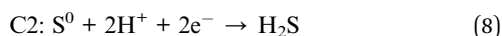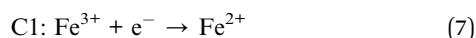

Fig. 3 Typical cyclic voltammogram profiles of CPE−without mineral(ɪ) and CPE−mineral(ɪɪ) in pH 4.2 SARs. (a) CPE−galena, (b) CPE−pyrite and (c) CPE−galena−pyrite. $E_i = E_{OC}$, $E_{\lambda a} = 0.9$ V, $E_{\lambda c} = -0.9$ V, $E_f = E_{OC}$, $v = 5$ mV S^{-1}. Where (a′) and (c′) are re-scaled versions of (a) and (c) at the same image, respectively.

826 | Environ. Sci.: Processes Impacts, 2018, 20, 822–832

This journal is © The Royal Society of Chemistry 2018

Biegler and Swift revealed that this peak corresponds to the oxidation of pyrite to ferric ions, sulfur and sulfate ions, as shown in reaction (6).[34]

$$A1: FeS_2 + (8 - 4x)H_2O \rightarrow$$
$$Fe^{3+} + xS^0 + (2 - x)SO_4^{2-} + (16 - 8x)H^+ + (15 - 6x)e^- \quad (6)$$
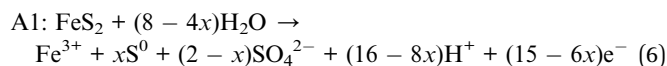
In the reverse scan, reduction of the surface products formed in the oxidation region occurs at peaks C1 (0.4 V) and C2 (−0.4 V), which correspond to the reduction of Fe^{3+} and S^0, as shown in reaction (7)[35] and reaction (8),[33–36] respectively. At a potential that is more negative than peak C2, another peak (C3) occurs at approximately −0.7 V, which is consistent with the results of Almeida and Giannetti, and peak C3 can be attributed to the reduction of pyrite, as indicated in reaction (9).[37] In an acidic environment, the FeS generated in reaction (9) was then dissolved in reaction (10).

$$C1: Fe^{3+} + e^- \rightarrow Fe^{2+} \quad (7)$$

$$C2: S^0 + 2H^+ + 2e^- \rightarrow H_2S \quad (8)$$

$$C3: FeS_2 + 2H^+ + 2e^- \rightarrow FeS + H_2S \quad (9)$$

$$FeS + 2H^+ = Fe^{2+} + H_2S \quad (10)$$

When the potential sweep is reversed at −0.8 V, the current swings positive at approximately 0.1–0.2 V, where the last anodic peak (A2) is observed. This peak is attributed to the oxidation of H_2S,[31,32] where H_2S is produced during the cathodic sweep, as shown in reactions (8)–(10).

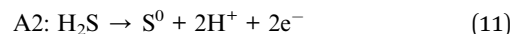$$A2: H_2S \rightarrow S^0 + 2H^+ + 2e^- \quad (11)$$

Fig. 2(c) shows the cyclic voltammogram obtained from the CPE–galena (75%, wt%)–pyrite with the sweep potential starting from the OCP. This cyclic voltammogram profile is similar to the galena voltammogram; however, the current density at the same potential is larger. These results indicate that the mixed and galena electrodes have the same oxidation and reduction processes. The addition of pyrite did not change the oxidative or reductive products of galena but increased the current density during the oxidation process. The results revealed that the presence of pyrite intensifies galena corrosion because of a galvanic effect between the galena and pyrite. Fig. 3 shows the voltammograms of the CPE containing PbS and/or FeS_2 in the pH 4.2 SAR solution. Compared to the results obtained in the pH 5.2 solution, the CPE–PbS and CPE–PbS–FeS_2 electrodes have similar voltammogram profiles, which reveals that the greater SAR acidity does not change their oxidation and reduction processes. However, compared to the results obtained in the pH 5.2 solution, the current densities of the CPE–PbS and CPE–PbS–FeS_2 electrodes at the same potential are larger, revealing that the greater SAR acidity facilitates the weathering of galena and galena with pyrite.

3.3 Polarization curve studies

The potentiodynamic curves of the CPE–galena and mixed mineral electrodes under the pH 5.2 and pH 4.2 SAR conditions are shown in Fig. 4. A comparison of the curves demonstrates that the galena and mixed mineral electrodes had similar potentiodynamic profiles. In both cases, the electrolyte solution at pH 5.2 is changed to 4.2, and the other electrode is galena mixed with pyrite. The potentiodynamic curve clearly shifted to the right and became more positive in both the x and y directions.

The Tafel extrapolation method was used to derive the corrosion potential E_{corr} and corrosion current density i_{corr}.[38] In addition, the polarization resistance (R_p) was estimated according to the Stern–Geary equation, $R_p = b_a b_c / [2.3 i_{corr}(b_a + b_c)]$,[39] and the polarization results are listed in Table 3.

By decreasing the pH value from 5.2 to 4.2, the E_{corr} values of the galena and mixed mineral electrodes increased from −77.2 to −7.8 mV and from 0.6 to 48.1 mV, respectively, and the i_{corr} values increased from 0.0052 to 0.12 μA cm^{-2} and 0.013 to 0.29 μA cm^{-2}, respectively. These results show that the increase in
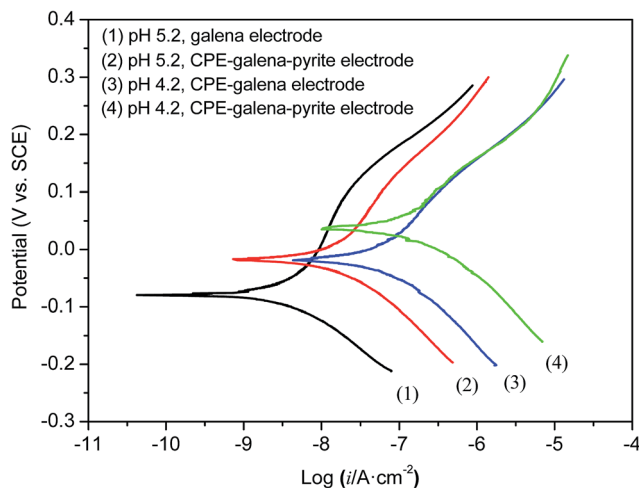

Fig. 4 Potentiodynamic curves of the CPE−galena and CPE−galena−pyrite electrodes in pH 5.2 and pH 4.2 SARs.

Table 3 Electrochemical parameters of the mineral electrodes at pH 5.2 and pH 4.2

Electrode	E_{corr} (mV)		i_{corr} (μA cm^{-2})		R_p (Ω cm^2)		v (g per m^2 per year)	
	pH 5.2	pH 4.2	pH 5.2	pH 4.2	pH 5.2	pH 4.2	pH 5.2	pH 4.2
CPE–PbS	−77.2	−7.8	0.0052	0.12	6910.0	244.1	1.7	39.6
CPE–PbS–FeS_2 (25%)	0.6	48.1	0.013	0.29	2219.3	92.3	4.3	95.7

This journal is © The Royal Society of Chemistry 2018

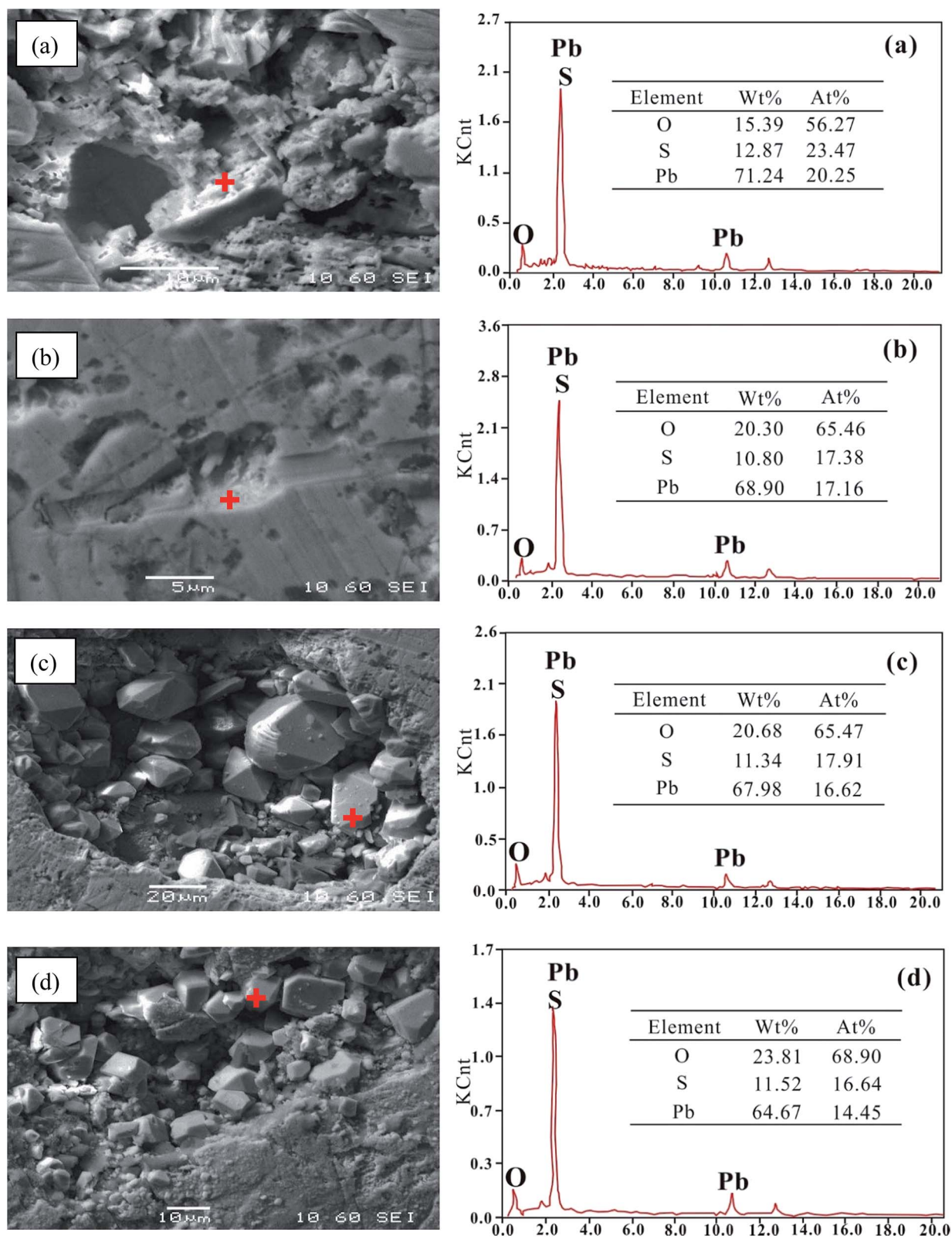*Environ. Sci.: Processes Impacts*, 2018, **20**, 822–832 | **827**

Fig. 5 SEM images and the corresponding EDS spectra of galena after 2 weeks of weathering in different SARs, where (a) pH 5.2, (b) pH 4.2, and (c) pH 5.2 coupled with pyrite powder and (d) pH 4.2 coupled with pyrite powder.

828 | *Environ. Sci.: Processes Impacts*, 2018, **20**, 822–832

This journal is © The Royal Society of Chemistry 2018

SAR acidity promoted the weathering of galena and galena–pyrite mixed minerals. Furthermore, the promotion efficiencies (η) for the galena and mixed mineral electrodes were 2208% and 2131%, respectively. In this study, η is defined as $\eta\% = (i_{corr} - i_{corr}^{0})/i_{corr}^{0} \times 100$, which is often used as the inhibition efficiency in materials science.[40–42] The SAR composition consists
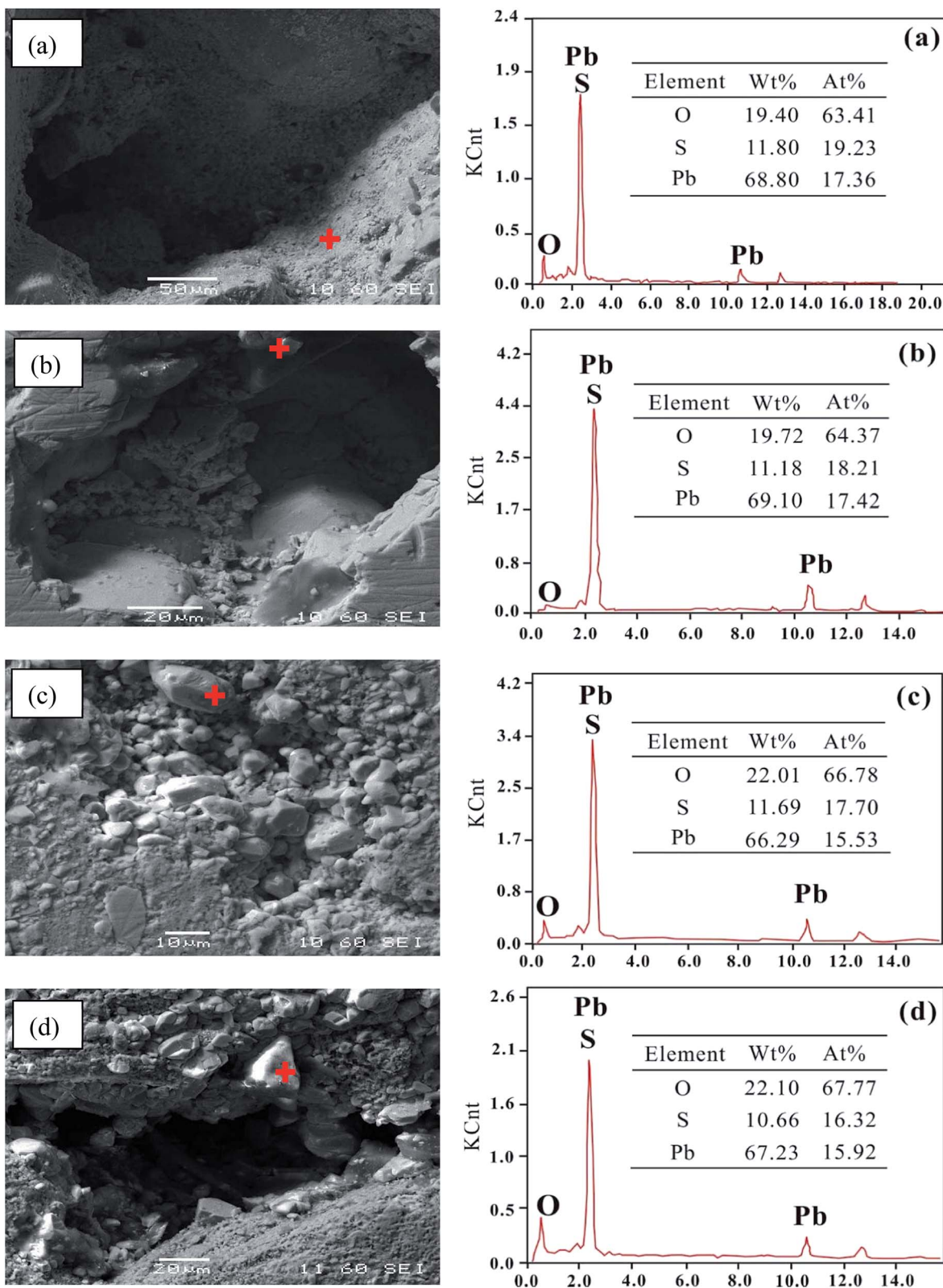

Fig. 6 SEM images and the corresponding EDS spectra of galena after 10 weeks of weathering in different SARs, where (a) pH 5.2, (b) pH 4.2, and (c) pH 5.2 coupled with pyrite powder and (d) pH 4.2 coupled with pyrite powder.

This journal is © The Royal Society of Chemistry 2018

Environ. Sci.: Processes Impacts, 2018, **20**, 822–832 | **829**

of several different non-oxidizing and non-reducing ions; therefore, the dissolved O_2 in the SAR is specified by the cathodic reaction (12), and the anodic reaction is indicated by A1 (reaction (1)). Clearly, an increase in H^+ benefits the cathodic reaction, which results in decreases in the polarization resistances of the galena and mixed electrodes from 6910.0 to 244.1 Ω cm^2 and 2219.3 to 92.3 Ω cm^2, respectively.

$$O_2 + 4H^+ + 4e^- \rightarrow 2H_2O \qquad (12)$$
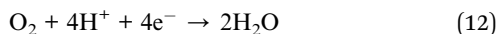
When the galena electrode contained pyrite, the E_{corr} values of the galena and mixed mineral electrodes increased from −77.2 to 0.6 mV and −7.8 to 48.1 mV, respectively, and the i_{corr} values increased from 0.0052 to 0.013 μA cm^{-2} and 0.12 to 0.29 μA cm^{-2}, respectively. The results show that the presence of pyrite promoted galena weathering, and the promotion efficiencies (η) for the galena and mixed mineral electrodes were 150% and 142%, respectively. This result is due to the galvanic effect described as follows. When galena and pyrite are in contact in a SAR medium, galvanic interactions occur, and a charge transfer is facilitated. The galvanic interaction changes the rates of the anodic and cathodic half-reactions that occur at the surface of each mineral.[27] As a result, the polarization resistance of galena decreased from 6910.0 to 2219.3 Ω cm^2 and from 244.1 to 92.3 Ω cm^2 in the pH 5.2 and pH 4.2 SAR solutions, respectively.

3.4 Surface analysis

Fig. 5 and 6 show the SEM images and EDS spectra, respectively, of the weathered galena surfaces after 2 weeks and 10 weeks. It is clear from the images that the weathered surfaces of the samples have corrosion holes. At both 2 weeks and 10 weeks, the weathered galena surfaces displayed lumpy or fluffy masses at pH 5.2, and this phenomenon was enhanced when the pH decreased to 4.2 without pyrite. When the galena contained pyrite (after 2 weeks or 10 weeks), the weathered galena surfaces exhibited crystal particles, which were confirmed as $PbSO_4$ by the EDS spectra.

Fig. 7 shows the Raman spectra of pristine and weathered galena samples. No peaks were observed from the pristine sample. After 2 weeks and 10 weeks, the weathered galena samples exhibited similar Raman spectra under the same SAR pH conditions; however, the intensity after 10 weeks of weathering was greater. In each Raman spectrum, broad Raman peaks are shown at 437–438, 600 and 960–969 cm^{-1}. These peaks are characteristic of a structure that includes lead sulfate species.[43,44] When galena is coupled with pyrite, the Raman spectra (Fig. 7(c) and (d)) show two new Raman peaks at 220 and 470 cm^{-1}, which are usually assigned to elemental sulfur (S^0).[45] The emergence of S^0 confirmed the initial galena weathering process and revealed that the galvanic effect promotes galena weathering, which results in a thicker S^0 film, and some of the S^0 does not have enough time to transform into SO_4^{2-}.
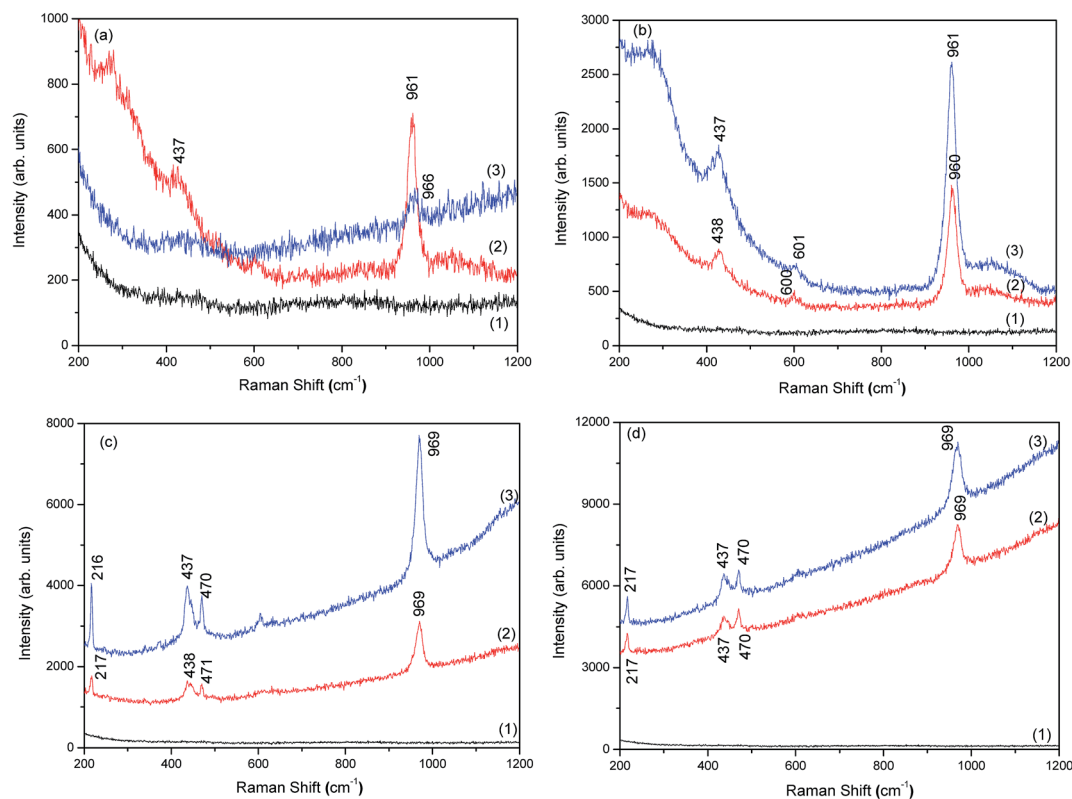

Fig. 7 Raman spectra of the massive galena electrodes after weathering in different SARs, where (a) pH 5.2, (b) pH 4.2, and (c) pH 5.2 coupled with pyrite powder and (d) pH 4.2 coupled with pyrite powder for: (1) a pristine surface, (2) 2 weeks leached surfaces and (3) 10 weeks leached surfaces.

830 | *Environ. Sci.: Processes Impacts*, 2018, **20**, 822–832

This journal is © The Royal Society of Chemistry 2018

Unfortunately, the $S_2O_3^{2-}$ Raman peak was not evident because $S_2O_3^{2-}$ is an unstable intermediate product.

4 Environmental assessments

Depending on the corrosion current density i_{corr}, we can get the galena weathering rate according to the Faraday equation $r = \dfrac{Mi_{corr}}{nF}$, where r is the weathering rate, g per m^2 per year, i_{corr} is the corrosion current density, μA cm^{-2}, M is the atomic weight, g mol^{-1}, n is the valence state, and F is the Faraday constant, 96 487C mol^{-1}. For example (Table 1), when the acid rain pH value was 5.2, and galena i_{corr} was 0.0052 μA cm^{-2} the galena weathering rate was 1.7 g per m^2 per year, that is, when the galena area is 1 m^2, it will release 1.7 g Pb^{2+} to solution in a year, and more Pb^{2+} ions would be released when the pH value of acid rain decreased to 4.2, that is 39.6 g per m^2 per year. When containing pyrite, galena i_{corr} would increase to 0.013 μA cm^{-2} at the acid rain pH of 5.2, suggesting that 4.3 g Pb^{2+} would be released in 1 year, and the released Pb^{2+} would reach 95.7 g per m^2 per year at the acid rain pH of 4.2. As above, if we know the galena component, and know acid rain ion concentrations and acidity, we can assess how many Pb^{2+} ions will be released in a certain time. On this basis, we can quantitatively evaluate to what extent acid rain affects soil Pb^{2+} pollution in a given field and in a certain time, if we know the content of galena in the soil and know the acid rain ion concentrations and acidity.

5 Conclusions

Under acid rain conditions, galena can be easily weathered, release Pb^{2+} and other heavy metal ions, causing environmental issues. This process, in nature, is an electrochemical process. *In situ* electrochemical technology and surface analysis technology were combined to investigate the galena weathering process under simulated acid rain conditions.

Cyclic voltammetry studies, SEM and Raman spectra analysis revealed that galena weathering in SAR could cause an initial increase in Pb^{2+} ions and result in the formation of a passive S^0 film. Then, at higher potentials, S^0 may be transformed into $S_2O_3^{2-}$, and the terminal product was SO_4^{2-}. The presence of pyrite did not change the galena corrosion mechanism, but it did change the corrosion intensity through galvanic interactions.

Increased acidity stimulates galena weathering. The galena corrosion current density (i_{corr}) increased from 0.0052 to 0.12 μA cm^{-2}, and the promotion efficiency η was 2208% as the pH of the SAR decreased from 5.2 to 4.2. In addition, the presence of pyrite is favourable for galena weathering. When the electrode contained 25% (wt%) pyrite, the galena i_{corr} increased from 0.0052 to 0.013 μA cm^{-2}, and η was 150%. Galena will release 1.7 g per m^2 per year Pb^{2+} to solution when the pH of acid rain is 5.2, and the released Pb^{2+} will reach 95.7 g per m^2 per year when the pH of acid rain is 4.2 plus the galvanic effect of pyrite.

Conflicts of interest

The authors declare no conflicts of interest.

References

1 U. A. Lar, C. S. Ngozi-Chika and E. C. Ashano, Human exposure to lead and other potentially harmful elements associated with galena mining at New Zurak, central Nigeria, *J. Afr. Earth Sci.*, 2013, **84**, 13–19.

2 R. Souissi, F. Souissi, M. Ghorbel, M. Munoz and P. Courjault-Radé, Heavy metals distribution and mobility in flotation tailings and agricultural soils near the abandoned Pb–Zn district of Jebel Hallouf-sidi Bouaoiane (NW Tunisia), *Environ. Earth Sci.*, 2015, **73**, 3501–3512.

3 A. Boughriet, P. Recourt, N. Proix, G. Billon, M. Leermakers, J. C. Fischer and B. Ouddane, Fractionation of anthropogenic lead and zinc in Deule River sediments, *Environ. Chem.*, 2007, **4**, 114–122.

4 R. A. Smith, *Air and Rain. The Beginnings of Chemical Climatology*, Longmans, Green, London, 1872.

5 J. Kuylenstierna, H. Rodhe, S. Cinderby and K. Hicks, Acidification in developing countries; ecosystem sensitivity and the critical load approach on a global scale, *Ambio*, 2001, **30**, 20–28.

6 L. Gimeno, E. Marín, T. D. Teso and S. Bourhim, How effective has been the reduction of SO$_2$ emissions on the effect of acid rain on ecosystems?, *Sci. Total Environ.*, 2001, **275**, 63–70.

7 Z. Dai, Y. Liu, X. Wang and D. Zhao, Changes in pH, CEC, and exchangeable acidity of some forest soils in southern China during the last 32–35 years, *Water, Air, Soil Pollut.*, 1998, **108**, 377–390.

8 C. D. Evans, J. M. Cullen, C. Alewell, J. Kopácek, A. Marchetto, F. Moldan, A. Prechtel, M. Rogora, J. Veselý and R. F. Wright, Recovery from acidification in European surface waters, *Hydrol. Earth Syst. Sci.*, 2001, **5**, 283–297.

9 B. L. Skjelkvale, J. Mannio, A. Wilander and T. Andersen, Recovery from acidification of lakes in Finland, Norway and Sweden 1990–1999, *Hydrol. Earth Syst. Sci.*, 2001, **5**, 327–337.

10 V. Kucera and S. Fitz, Direct and indirect air pollution effects on materials including cultural monuments, *Water, Air, Soil Pollut.*, 1995, **85**, 153–165.

11 WHO (World Health Organization), *1995, Update and Revision of the Air Quality Guidelines for Europe. Meeting of the Working Group 'Classical'Air Pollutants*, Bilthoven, The Netherlands, October 1994, pp. 11–14.

12 S. Y. Xie, R. B. Wang and H. H. Zheng, Analysis on the acid rain from 2005 to 2011 in China, *Monitor Forewarning*, 2012, **4**, 33–37.

13 Z. Dang, C. Q. Liu and J. H. Martin, Mobility of heavy metals associated with the natural weathering of coal, *Environ. Pollut.*, 2002, **118**, 419–426.

14 J. Smuda, D. Bernhard, F. Kurt, M. Peter and G. Walter, Mineralogical and geochemical study of element mobility at the sulfide-rich Excelsior waste rock dump from the polymetallic Zn–Pb–(Ag–Bi–Cu) deposit, Cerro de Pasco, *J. Geochem. Explor.*, 2007, **92**, 97–110.

15 C. A. Chavez, S. M. Erick, L. Gilles, M. T. Carolina, P. A. Ofelia and G. Tammie, Geochemistry and mineralogy of mine-waste material from a "skarn-type" deposit in central Mexico: Modeling geochemical controls of metals in the surface environment, *J. Geochem. Explor.*, 2014, **144**, 28–36.

16 Z. H. Ding, Q. Y. Wang and X. Hu, Fractionation of Zn and Pb in bulk soil and size fractions of water-stable micro-aggregates of Lead/Zinc tailing soil under simulated acid rain, *Procedia Environ. Sci.*, 2011, **10**, 325–330.

17 L. Yuan and Y. S. Liu, The leaching principles of heavy metals in lead and zinc tailings in simulation acid rain, *Environ. Eng.*, 2012, **30**, 586–590.

18 S. G. Salamy and J. G. Nixon, The application of electrochemical methods to flotation research, *Inst. Min. Metall.*, 1953, 503.

19 D. T. Sawyer and J. L. Roberts, *Experimental Electrochemistry for Chemists*, Wiley, 1974.

20 R. L. Paul, M. J. Nicol, J. W. Diggle and A. P. Saunders, The electrochemical behaviour of galena lead sulphide: I. Anodic dissolution, *Electrochim. Acta*, 1978, **23**, 625–633.

21 H. R. Lara, B. Roberto, G. Marcos, M. Martine, H. Bernard, D. Manuel, M. N. Ghinwa and C. Roel, Galena weathering under simulated calcareous soil conditions, *Sci. Total Environ.*, 2011, **409**, 3971–3979.

22 I. Lazaro, N. Martinez-Medina, I. Rodriguez, E. Arce and I. Gonzalez, The use of carbon paste electrodes with non-conducting binder for the study of minerals: chalcopyrite, *Hydrometallurgy*, 1995, **38**, 277–287.

23 C. H. An, Acid rain and its control in Dongchuan, *Environ. Sci. Survey*, 2015, **34**, 45–49.

24 E. T. Pecina, A. Uribe, J. A. Finch and F. Nava, Mechanism of di-isobutyl dithiophosphinate adsorption onto galena and pyrite, *Miner. Eng.*, 2006, **19**, 904–911.

25 E. Ahlberg and J. Ásbjörnsson, Carbon paste electrodes in mineral processing: an electrochemical study of galena, *Hydrometallurgy*, 1993, **34**, 175–185.

26 K. A. Natarajan and I. Iwasaki, Eh/pH response of noble metal and sulphide mineral electrode, *Trans. Am. Inst. Min. Metall. Eng.*, 1972, **252**, 437–439.

27 P. R. Holmes and F. K. Crundwell, Kinetic aspects of galvanic interactions between minerals during dissolution, *Hydrometallurgy*, 1995, **39**, 353–375.

28 J. R. Gardner and R. Woods, A study of the surface oxidation of galena using cyclic voltammetry, *Chem. Informationsdienst*, 1979, **10**, 447–459.

29 I. Cisneros-González, M. T. Oropeza-Guzmán and I. González, An electrochemical study of galena concentrate in perchlorate medium at pH 2.0: the influence of chloride ions, *Electrochim. Acta*, 2000, **45**, 2729–2741.

30 M. V. B. C. Almeida and F. B. Giannetti, The electrochemical behavior of pyrite–pyrrhotite mixtures, *J. Electroanal. Chem.*, 2003, **553**, 27–34.

31 J. L. Nava, M. T. Oropeza and I. González, Electrochemical characterization of sulfur species formed during anodic dissolution of galena concentrate in perchlorate medium at pH 0, *Electrochim. Acta*, 2002, **47**, 1513–1525.

32 P. Sivenas and F. R. Foulkes, Cathodic reactions of natural galena in perchloric acid, *Electrochim. Acta*, 1984, **29**, 1215–1223.

33 I. C. Hamilton and R. Woods, An investigation of surface oxidation of pyrite and pyrrhotite by linear potential sweep voltammetry, *J. Electroanal. Chem. Interfacial Electrochem.*, 1981, **118**, 327–343.

34 T. Biegler and D. A. Swift, Anodic behaviour of pyrite in acid solutions, *Electrochim. Acta*, 1979, **24**, 415–420.

35 E. Ahlberg and A. E. Broo, Electrochemical reaction mechanisms at pyrite in acidic perchlorate solutions, *J. Electrochem. Soc.*, 1997, **144**, 1281–1286.

36 Q. Yin, G. H. Kelsall, D. J. Vaughan and N. J. Welham, Rotating Ring (Pt)–Disc (FeS$_2$) Electrode Behavior in Hydrochloric Solutions, *J. Colloid Interface Sci.*, 1999, **210**, 375–383.

37 C. M. V. B. Almeida and B. F. Giannetti, Comparative study of electrochemical and thermal oxidation of pyrite, *J. Solid State Electrochem.*, 2002, **6**, 111–118.

38 A. J. Bard and L. R. Faulkner, *Electrochemical methods: fundamentals and applications*, Wiley and Sons, Hoboken, 2nd edn, 2001.

39 M. Stern and A. L. Geary, Electrochemical polarization. 1. A theoretical analysis of the shape of polarization curves, *J. Electrochem. Soc.*, 1957, **104**, 56–63.

40 R. Solmaz, G. Kardaş, B. Yazici and M. Erbil, Adsorption and corrosion inhibitive properties of 2-amino-5-mercapto-1,3,4-thiadiazole on mild steel in hydrochloric acid media, *Colloids Surf., A*, 2008, **312**, 7–17.

41 X. Wang, H. Yang and F. Wang, An investigation of benzimidazole derivative as corrosion inhibitor for mild steel in different concentration HCl solutions, *Corros. Sci.*, 2001, **53**, 113–121.

42 C. Verma, M. A. Quraisih and A. Singh, 2-Amino-5-nitro-4,6-diarylcyclohex-1-ene-1,3,3-tricarbonitriles as new and effective corrosion inhibitors for mild steel in 1 M HCl: Experimental and theoretical studies, *J. Mol. Liq.*, 2015, **212**, 804–812.

43 J. G. Shapter, M. H. Brooker and W. M. Skinner, Observation of the oxidation of galena using Raman spectroscopy, *Int. J. Miner. Process.*, 2000, **60**, 199–211.

44 K. Eremin, J. Stenger and M. L. Green, Raman spectroscopy of Japanese artists' materials: the tale of Genji by Tosa Mitsunobu, *J. Raman Spectrosc.*, 2006, **37**, 19–24.

45 K. Sasaki, M. Tsunekawa, T. Ohtsuka and H. Konno, The role of sulfuroxidizing bacteria Thiobacillus thiooxidans in pyrite weathering, *Colloids Surf., A*, 1998, **133**, 269–278.